



Contents lists available at ScienceDirect

Radiation Measurements

journal homepage: www.elsevier.com/locate/radmeas

A tunneling model for afterglow suppression in CsI:Tl,Sm scintillation materials

L.A. Kappers^{a,*}, R.H. Bartram^a, D.S. Hamilton^a, A. Lempicki^b, C. Brecher^b, V. Gaysinskiy^c, E.E. Ovechkina^c, S. Thacker^c, V.V. Nagarkar^c^a Department of Physics, University of Connecticut, 2152 Hillside Road, Storrs, CT 06269-3046, USA^b ALEM Associates, 303 Commonwealth Avenue, Boston, MA 02115, USA^c Radiation Monitoring Devices (RMD) Inc., 44 Hunt St., Watertown, MA 02472, USA

ARTICLE INFO

Article history:

Received 7 August 2009

Received in revised form

4 September 2009

Accepted 9 November 2009

Keywords:

Cesium Iodide

Afterglow

Tunneling

ABSTRACT

Combined radioluminescence, afterglow and thermoluminescence experiments on single-crystal samples of co-doped CsI:Tl,Sm suggest that samarium electron traps scavenge electrons from thallium traps and that electrons subsequently released by samarium recombine non-radiatively with trapped holes, thus suppressing afterglow. Experiments on single crystals support the inference that electrons tunnel freely between samarium ions and are trapped preferentially as substitutional Sm^+ near $V_{\text{KA}}(\text{Tl}^+)$ centers where non-radiative recombination is the rate-limiting step. Afterglow in microcolumnar films of CsI:Tl,Sm is enhanced by inhomogeneities which impede tunneling between samarium ions, but is partly suppressed by annealing.

© 2009 Elsevier Ltd. All rights reserved.

1. Introduction

The feasibility of substantially diminishing afterglow in CsI:Tl scintillator material by co-doping with Sm^{2+} has been demonstrated (Nagarkar et al., 2008). Rate equations informed by experiment predict that deeper samarium electron traps scavenge electrons from shallower thallium traps and combined radioluminescence, afterglow and thermoluminescence experiments on single-crystal samples suggest that electrons released by Sm^+ recombine non-radiatively with holes trapped as $V_{\text{KA}}(\text{Tl}^+)$ centers, thus suppressing afterglow (Bartram et al., 2008). A linear-coupling model in the harmonic approximation, based on quantum-chemistry calculations with selective lattice relaxation, suggests further that non-radiative charge transfer is enabled by low-energy excited states of Sm^{2+} within the ground configuration and is mediated by spin-orbit interaction. Although recombination is predominantly non-radiative, tracking of the process with enhanced gain settings is enabled both by radiative recombination following thermal ionization and by a small radiative component of the charge-transfer recombination associated with magnetic-dipole transitions from low-energy excited states of Sm^{2+} . In the present investigation, combined scintillation and afterglow experiments were performed on two single-crystal samples of CsI:Tl,Sm with

nominal concentrations of 0.11% Tl^+ and of 0.2% and 0.05% Sm^{2+} , respectively, in order to determine the concentration dependence of the rate of non-radiative charge transfer. Co-doping of CsI:Tl with Sm^{2+} also diminishes the scintillation light output somewhat; that effect has been discussed extensively in previous work (Nagarkar et al., 2008). Two microcolumnar films of CsI:Tl,Sm, grown by vapor deposition on a graphite substrate with equal 0.1% nominal concentrations of Tl^+ and Sm^{2+} , one of which was annealed for 48 h at +250 °C, were also investigated by combined scintillation and thermoluminescence. The purpose of these films is to enhance the spatial resolution of radiation detectors, but afterglow suppression is appreciably less effective than in single crystals, although it is partly restored by annealing.

2. Experiment

An electron Van de Graaff accelerator operated at a beam voltage of 1.0 MV was employed as the primary radiation source with the 1.0 μA electron beam stopped by a thin copper target that served as a point source of 0.5 MeV gamma rays. Samples were mounted on a heated pedestal and cooled by flowing nitrogen gas, the sample temperature was monitored by a thermocouple and luminescence was transmitted to a photomultiplier by a shielded optical fiber. Immediately following four-minute irradiations the gain was increased by several orders of magnitude to monitor afterglow of single crystals or thermoluminescence of microcolumnar films. Light output data were recorded at four-second intervals.

* Corresponding author. Tel.: +1 860 486 4782/+1 860 684 3591; fax: +1 860 486 3346.

E-mail address: lawrence.kappers@uconn.edu (L.A. Kappers).

3. Rate equations

Complete rate equations for each phase of the process were presented previously (Bartram et al., 2008). Rate equations for the afterglow phase in terms of the normalized trapped-hole concen-

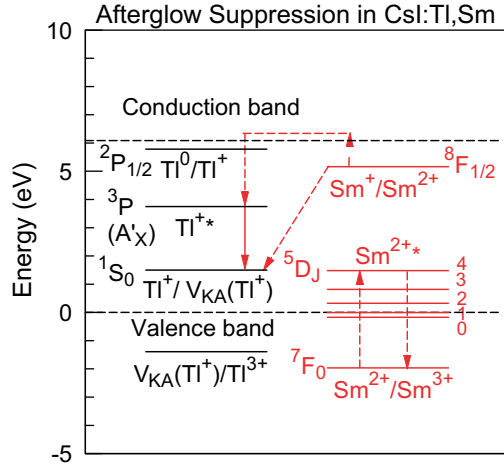


Fig. 1. Energy-level diagram illustrating the mechanism for afterglow suppression in CsI:Tl,Sm by non-radiative charge-transfer transitions.

tration \tilde{n}_h and normalized light output \tilde{I} are

$$\frac{d\tilde{n}_h}{dt} \equiv -p_e^{(Sm)} \tilde{n}_h - \alpha \tilde{n}_h^2, \quad (1)$$

$$\tilde{I} \equiv -\frac{d\tilde{n}_h}{dt} - (1-r)\alpha \tilde{n}_h^2 = r\alpha \tilde{n}_h^2 + p_e^{(Sm)} \tilde{n}_h, \quad (2)$$

$$\alpha \equiv s_A \exp(-E_A/k_B T), \quad (3)$$

$$p_e^{(Sm)} \equiv s^{(Sm)} \exp(-E^{(Sm)}/k_B T), \quad (4)$$

with explicit solution for fixed T :

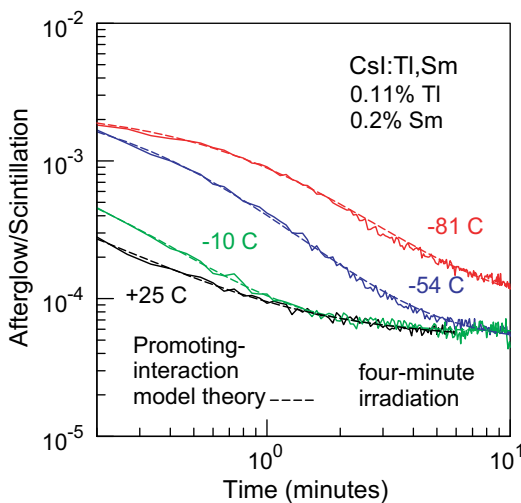


Fig. 2. Recorded ratio of afterglow and scintillation for the single-crystal sample with 0.2% Sm^{2+} following four-minute irradiations at four temperatures (continuous curves) compared with theory with the fitted parameters listed in Table 1 plus additive constants to simulate PM shot noise (dashed curves).

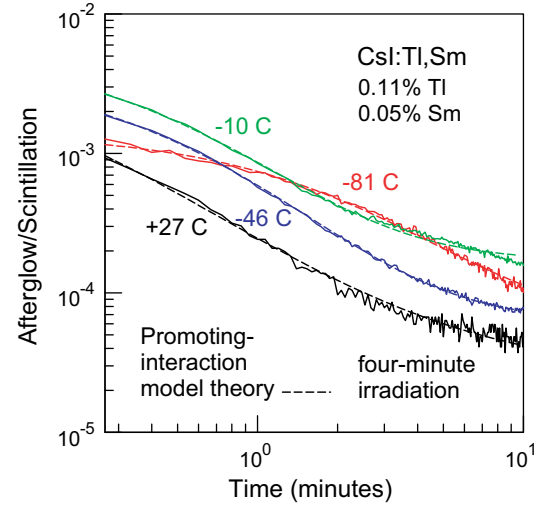


Fig. 3. Recorded ratio of afterglow and scintillation for the single-crystal sample with 0.05% Sm^{2+} following four-minute irradiations at four temperatures (continuous curves) compared with theory with the fitted parameters listed in Table 1 plus additive constants to simulate PM shot noise (dashed curves).

$$\tilde{n}_h \equiv \frac{\tilde{n}_{h0} \exp(-p_e^{(Sm)} t)}{1 + (\alpha \tilde{n}_{h0} / p_e^{(Sm)}) [1 - \exp(-p_e^{(Sm)} t)]}. \quad (5)$$

The parameters α and r respectively determine the rate of charge-transfer recombination and its radiative fraction, and the parameter $p_e^{(Sm)}$ determines the rate of thermal ionization. These equations were fitted to afterglow data with the optimized parameter values listed in Table 1. Optimized values of r are typically $\sim 1\%$. Figs. 1–5.

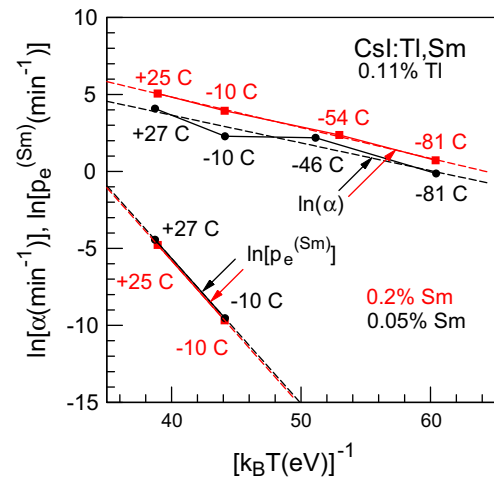


Fig. 4. Comparison of $\ln(\alpha)$ and $\ln(p_e^{(Sm)})$ as functions of $1/k_B T$ (continuous curves) with Eqs. (3) and (4) (dashed curves) and the optimized parameters listed in Table 1.

Table 1
Optimized parameters for thermal activation.

% Sm^{2+}	E_A (eV)	s_A (min^{-1})	$E^{(Sm)}$ (eV)	$s^{(Sm)}$ (min^{-1})
0.2	0.199	3.66×10^5	0.946	8.46×10^{13}
0.05	0.180	5.26×10^4	0.925	8.48×10^{13}

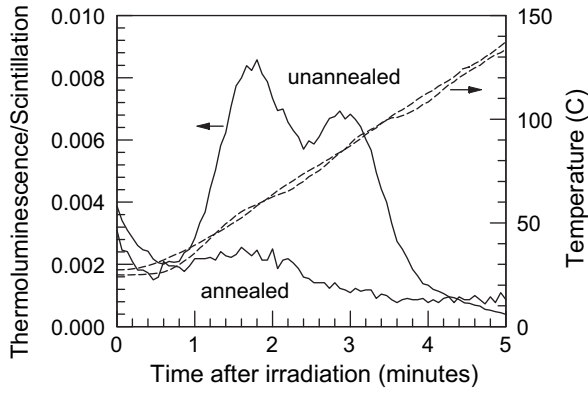


Fig. 5. Normalized thermoluminescence (continuous curves) and sample temperatures (dashed lines) of CsI:Tl,Sm microcolumnar films with equal nominal 0.1% concentrations of Tl⁺ and Sm²⁺, one annealed for 48 h at +250 °C and one unannealed, following four-minute irradiations at room temperature.

4. Promoting-interaction model

The frequency factor s_A is proportional to the promoting-interaction and thus to the square of the matrix element of the spin-orbit interaction between initial and final states. A diffuse 6s orbital centered at \vec{r}_0 can be represented in a continuum approximation with effective mass ratio $m^*/m \approx 1.0$ by

$$\phi_{6s}(\Delta r) = \frac{\exp(-\Delta r/\kappa a_0)}{\pi^{1/2}(\kappa a_0)^{3/2}}, \Delta r \equiv |\vec{r} - \vec{r}_0| \quad (6)$$

$$\frac{s_{A1}}{s_{A2}} = \left[\frac{\phi_{6s}(\Delta r_1)}{\phi_{6s}(\Delta r_2)} \right]^2 = \exp[2(\Delta r_2 - \Delta r_1)/\kappa a_0], \quad (7)$$

With the assumption of a fixed separation Δr of initial and final sites in each crystal sample, the ratio of promoting-interactions is given by

$$\frac{\Delta r_2}{\Delta r_1} = \frac{\rho_1^{1/3}}{\rho_2^{1/3}} = 1.25, \quad (8)$$

where ρ is the total dopant concentration and $\kappa = 6.31$ (David R. Lide, 1996). It follows that $\Delta r_1/a = 2.88$ and $\Delta r_2/a = 3.59$, where $a = 4.56 \text{ \AA}$ is the lattice parameter.

5. Discussion

The calculated values for the separation of initial and final sites are plausible for the nearest dopant sites but not for a random distribution of trapped charges substantially less than the dopant concentration. Accordingly, the promoting-interaction model incorporates the assumption that electrons tunnel freely between samarium ions and are trapped preferentially near $V_{KA}(\text{Tl}^+)$ centers where non-radiative recombination is the rate-limiting step, thus explaining the single non-radiative transition rate for fixed temperature and dopant concentration. An earlier tunneling model (Delbecq et al., 1974) provides an egregiously poor fit to the present data.

Acknowledgments

We thank NIH and DOE for support of this work under Grants No. R43 RR022921-01 and DE FG02 06ER84434, respectively.

References

- Bartram, R.H., Kappers, L.A., Hamilton, D.S., Lempicki, A., Brecher, C., Gaysinskiy, V., Ovechkina, E.E., Nagarkar, V.V., 2008. Afterglow suppression and non-radiative charge-transfer in CsI: Tl, Sm. IEEE Transactions on Nuclear Science 55, 1232–1236.
- Lide, David R. (Ed.), 1996. CRC Handbook of Chemistry and Physics, seventy seventh ed. CRC Press, Boca Raton, pp. 12–47.
- Delbecq, C.J., Toyozawa, Y., Yuster, P., 1974. Tunneling recombination of trapped electrons and holes in KCl:AgCl and KCl:TlCl. Physical Review B 9, 4497.
- Nagarkar, V.V., Brecher, C., Ovechkina, E.E., Gaysinskiy, V., Miller, S.R., Thacker, S., Lempicki, A., Bartram, R.H., 2008. Scintillation properties of CsI: Tl crystals codoped with Sm²⁺. IEEE Transactions on Nuclear Science 55, 1270–1274.